Title

Ras pathway inhibition prevents neovascularization by repressing endothelial cell sprouting

Journal

Journal of Clinical Investigation, 123(11)

ISSN

0021-9738

Authors

Westenskow, Peter D

Kurihara, Toshihide

Aguilar, Edith

et al.

Publication Date

2013-11-01

DOI

10.1172/jci70230

Peer reviewed

Ras pathway inhibition prevents neovascularization by repressing endothelial cell sprouting

Peter D. Westenskow,[1] Toshihide Kurihara,[1] Edith Aguilar,[1] Elizabeth L. Scheppke,[1] Stacey K. Moreno,[1] Carli Wittgrove,[1] Valentina Marchetti,[1] Iacovos P. Michael,[2] Sudarshan Anand,[3] Andras Nagy,[2] David Cheresh,[3] and Martin Friedlander[1]

[1]Department of Cell and Molecular Biology, The Scripps Research Institute, La Jolla, California, USA. [2]Samuel Lunenfeld Research Institute, Mount Sinai Hospital, Toronto, Ontario, Canada. [3]Department of Pathology, UCSD, San Diego, California, USA.

Vascular networks develop from a growing vascular front that responds to VEGF and other guidance cues. Angiogenesis is required for normal tissue function, but, under conditions of stress, inappropriate vascularization can lead to disease. Therefore, inhibition of angiogenic sprouting may prevent neovascularization in patients with blinding neovascular eye diseases, including macular degeneration. VEGF antagonists have therapeutic benefits but also can elicit off-target effects. Here, we found that the Ras pathway, which functions downstream of a wide range of cytokines including VEGF, is active in the growing vascular front of developing and pathological vascular networks. The endogenous Ras inhibitor p120RasGAP was expressed predominately in quiescent VEGF-insensitive endothelial cells and was ectopically downregulated in multiple neovascular models. MicroRNA-132 negatively regulated p120RasGAP expression. Experimental delivery of α-miR-132 to developing mouse eyes disrupted tip cell Ras activity and prevented angiogenic sprouting. This strategy prevented ocular neovascularization in multiple rodent models even more potently than the VEGF antagonist, VEGF-trap. Targeting microRNA-132 as a therapeutic strategy may prove useful for treating multiple neovascular diseases of the eye and for preventing vision loss regardless of the neovascular stimulus.

Introduction

Angiogenesis and maintenance of a normal vasculature is crucial to the function of all tissues but is particularly critical in the retina where oxygen concentrations and metabolic demands are the highest in the body. Under conditions of hypoxia and/or inflammation, proangiogenic factors stimulate pathological angiogenesis; this leads to hemorrhage and abnormalities in vascular permeability. These changes can obscure the visual axis and lead to uncontrolled gliosis and associated fibrovascular scarring that contribute to visual loss. Notable examples include diabetic retinopathy and age-related macular degeneration, the global leading causes of vision loss in industrialized nations. Elevated levels of VEGF are associated with pathological angiogenesis in these conditions, and VEGF antagonists are now widely used to treat neovascularization associated with diabetic retinopathy and age-related macular degeneration. While VEGF antagonism can prevent vision loss in a subset of patients with neovascular eye disease, many patients do not respond to therapy and some experience progressive photoreceptor and vascular loss (1, 2) as well as renal complications (3). Novel treatments for neovascularization that circumvent these problems may be developed only as more regulatory pathways that control angiogenesis are better understood or identified.

Normal and pathological vascular networks are generated from filopodia-bearing endothelial cells that explore their microenvironments in response to migratory cues (4, 5). In contrast, quiescent endothelial cells lack filopodia and are far less sensitive to VEGF-mediated activation (6). Several pathways that regulate endothelial cell sprouting have been identified, including Notch/Delta-like ligand 4, Netrin/Netrin receptor UNC5B, and VEGF/VEGFR2 (5, 7–10). Since Ras in endothelial cells acts downstream of VEGF as well as other growth factors that control angiogenesis (11), we hypothesized that it may also exert a significant role in regulating angiogenic sprouting and quiescence in endothelial cells. The Ras/Raf/MEK/ERK pathway can be inactivated by high levels of the GTPase p120RasGAP (12), and mutations in the p120RasGAP gene (*Rasa1*) induce severe defects in development of the murine vascular system (13). In humans, *RASA1* mutations induce hypervascularization and capillary malformations associated with arteriovenous malformation, arteriovenous fistula, or Parkes-Weber syndrome (14–16); we hypothesize that these defects are observed due to Ras hyperactivity.

In this study, we demonstrate that the activation status of the vascular endothelial Ras pathway can be used to distinguish sprouting and quiescent endothelial cells. We also observed that p120RasGAP expression levels are downregulated in multiple murine models of pathological ocular angiogenesis. Experimentally potentiating p120RasGAP expression levels using an antagomir to microRNA-132 (miR-132) promoted quiescence and prevented neovascularization. Therefore, the Ras pathway may be targeted selectively in the growing angiogenic front to prevent neovascularization and its complications in multiple neovascular eye diseases.

Results

The Ras pathway is active in the advancing angiogenic front. To test our hypothesis that the Ras pathway is involved in the regulation of endothelial cell sprouting, we examined the expression patterns of Ras signaling elements in retinal endothelial cells in several

Authorship note: Peter D. Westenskow and Toshihide Kurihara contributed equally to this work.

Conflict of interest: The authors have declared that no conflict of interest exists.

Citation for this article: *J Clin Invest.* 2013;123(11):4900–4908. doi:10.1172/JCI70230.

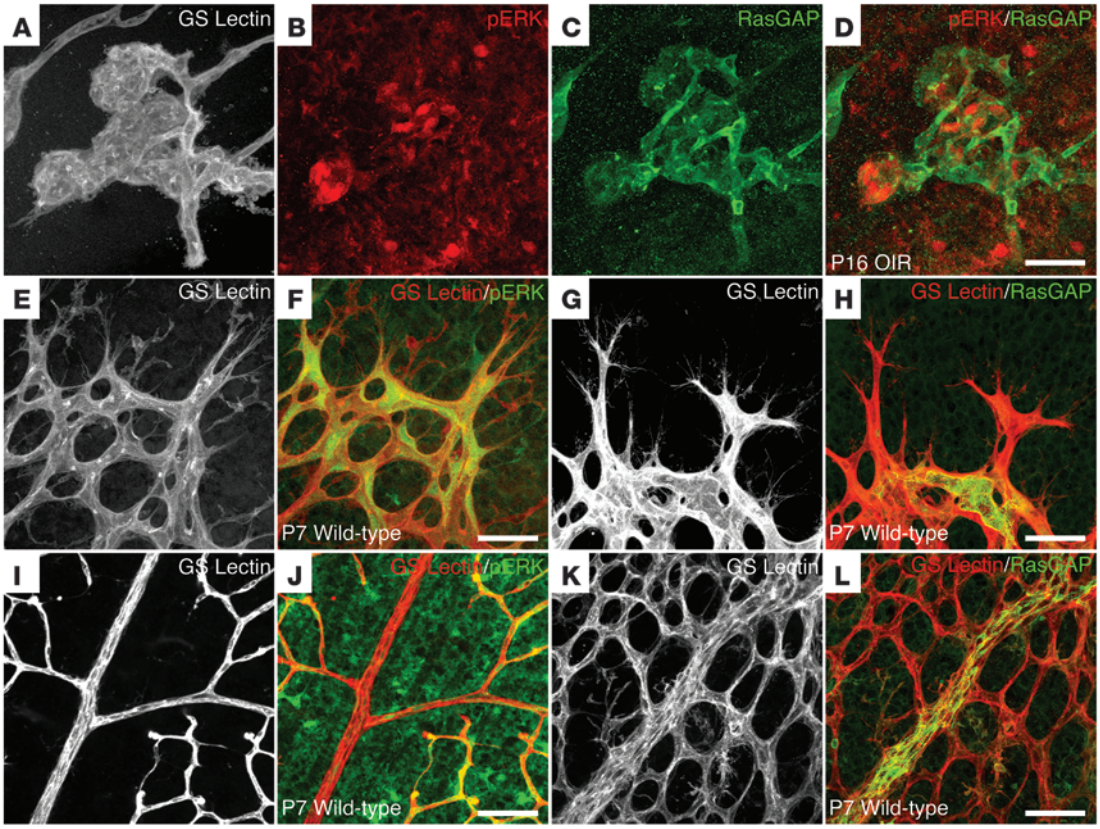

Figure 1

pERK specifically labels sprouting endothelial cells. (**A**) A representative GS lectin–stained neovascular tuft from a OIR retina staged on P16. (**B**) pERK-positive (red) and (**C**) p120RasGAP-positive (green) cells are observed in distinct compartments of the tuft. (**D**) Merged file. (**E**) In P7 wild-type flat-mounted retinas, the advancing vascular front is labeled with GS lectin. (**F**) pERK is readily detectable in the endothelial cells of the sprouting angiogenic front (green) of the GS lectin–labeled vascular network (red). (**G** and **H**) Conversely, p120RasGAP is only sporadically detected in GS lectin–labeled sprouting endothelial cells. (**I**) Central mature vessels were also examined after GS lectin labeling in P7 wild-type retinas. (**J**) pERK is not detected in the quiescent cells of central arteries or veins, but (**K** and **L**) p120RasGAP is highly expressed in both. Scale bars: 50 μm.

models of ocular neovascularization. In the oxygen-induced retinopathy (OIR) model, mouse pups are exposed to 75% oxygen for 5 days starting at P7 (17). In response to hyperoxia, dramatic vascular remodeling occurs and vessels in the central region of the superficial plexus are obliterated. Upon reexposure to normal oxygen levels (~20%) at P12, the avascular central retina becomes hypoxic; this stimulus drives neovascularization across the superficial vascular plexus.

Retinal whole mounts from OIR mice were prepared and immunolabeled with antibodies for phosphorylated ERK (pERK) and p120RasGAP. At P14, pERK- and p120RasGAP-positive cells could be observed in a mosaic and nonoverlapping pattern in the *Griffonia simplicifolia* (GS) lectin–labeled actively sprouting neovascular tufts (Figure 1, A–D). VEGFR2, a known tip cell marker, has a virtually identical expression pattern to that of pERK in OIR mice (Supplemental Figure 1, A–C; supplemental material available online with this article; doi:10.1172/JCI70230DS1). To confirm that pERK labels sprouting endothelial cells preferentially, we examined their expression in developing retinas. In retinas staged at P7, pERK was readily expressed in the sprouting endothelial cells of the nascent vascular network that is expanding toward the periphery of the eye (Figure 1, E and F). p120RasGAP, however, was detected only in scattered cells of the angiogenic front (Figure 1, G and H). Interestingly, the spatial expression of p120RasGAP was analogous to that of UNC5B, which is activated in tip cells and associated with inhibition of vascular sprouting (Supplemental Figure 1, D–F, and ref. 18). pERK was not observed in quiescent endothelial cells of central vessels (Figure 1, I and J), yet both p120RasGAP and UNC5B were readily detectable (Figure 1, K and L, and Supplemental Figure 1, G–J) in the same temporal and spatial patterns in both the arteries and veins. During retinal development, the temporal and spatial expression of p120RasGAP was consistent with normal patterning of the retinal vasculature (Supplemental Table 1), and, in adult mice, p120RasGAP was detected in all retinal vessels of all 3 plexus layers (Supplemental Figure 2). These data suggest that p120RasGAP may become activated during angiogenesis to inhibit endothelial cell sprouting and to promote quiescence.

We then reexamined pERK/p120RasGAP expression in OIR mice at multiple time points. At P12, when the nascent vasculature was being vaso-obliterated (and not sprouting), p120RasGAP was detected in the retinal vessels (Figure 2, A and B). However, in retinas staged at P14 to P16, when hypoxia was driving neovascular tuft formation, p120RasGAP was virtually undetectable (Figure 2, C–F). At P18 (a day after the number and size of the tufts reach maximal levels and spontaneous regression begins), high levels

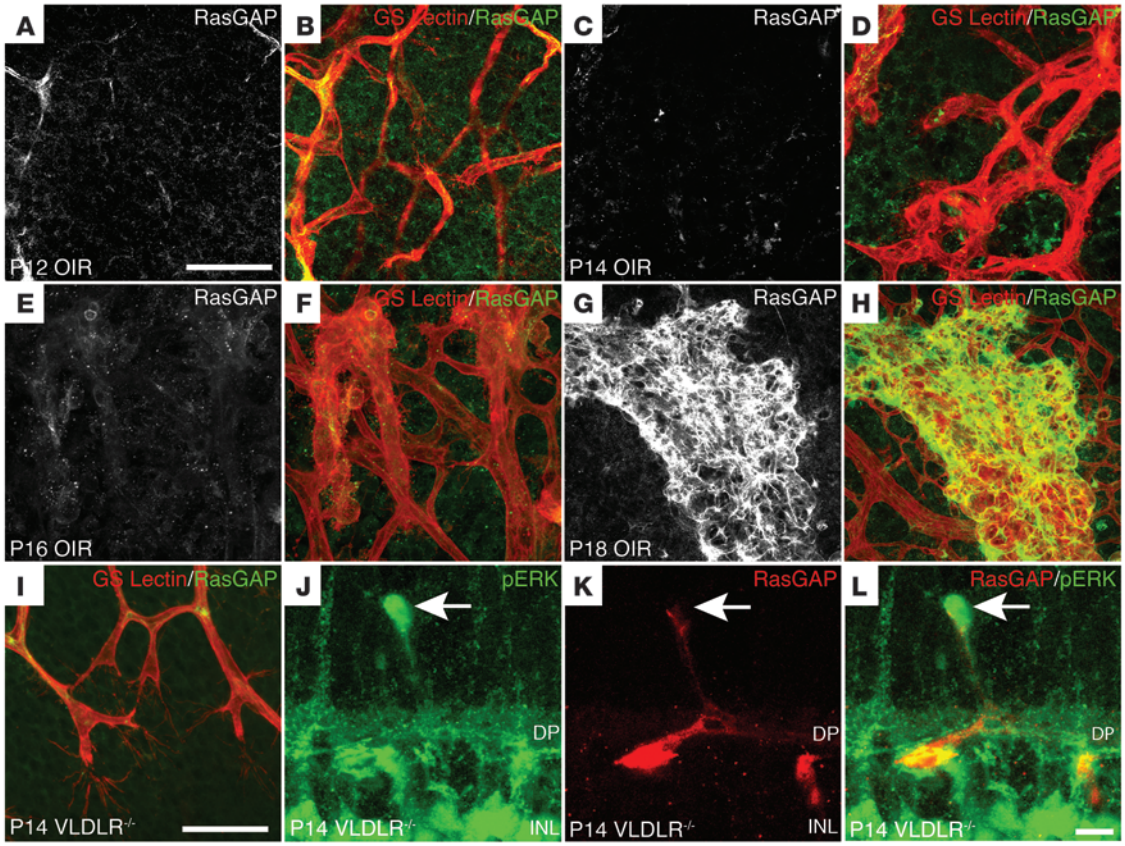

Figure 2

The Ras pathway is aberrantly active in OIR and *Vldlr*$^{-/-}$ mice. (**A**) In P12 OIR mice, p120RasGAP (white) is detected in the retinal vessels of the superficial plexus. (**B**) p120RasGAP (green) was overlaid with red GS lectin to label the vasculature. (**C**–**F**) At P14 and P16, it is barely detectable in neovascular regions. (**G** and **H**) At P18, p120RasGAP is abundantly expressed in the neovascular tufts. (**I**) Tip cells devoid of p120RasGAP are identifiable in the deep plexus in flat-mounted P14 *Vldlr*$^{-/-}$ retinas. (**J**) In thick-cut cross-sections, pERK is detected in the tip cell of the developing angioma (arrow) and in cells in the inner nuclear layer, and (**K**) p120RasGAP is very weakly expressed in the tip cell but is detectable in the endothelial cells of the deep plexus (DP). (**L**) A merged file is shown in. Scale bars: 50 μm (**A**–**I**); 10 μm (**J**–**L**).

of p120RasGAP were observed (Figure 2, G and H). The abrupt upregulation of p120RasGAP reflects a change in endothelial cell functionality, as the endothelial cells in the tufts stop sprouting.

The VLDL receptor (VLDLR) knockout mouse serves as a model for idiopathic juxtafoveal macular telangiectasia (MacTel) and retinal angiomatous proliferation (19–21). In this model, vessels sprouted aberrantly into the outer retina to form angiomas and neovascular tufts at the photoreceptor outer segment/retinal pigment epithelium (photoreceptor outer segment/RPE) interface (Figure 2I), occasionally also forming retinal/choroidal anastomoses. In these mice, pERK was detected in the sprouting endothelial cells of the invading angiomas (Figure 2, J and L), and p120RasGAP was nearly undetectable (Figure 2, K and L). Conversely, in wild-type mice, pERK was undetectable (Supplemental Figure 3, A and B), and high levels of p120RasGAP and UNC5B were observed in the deep plexus at these stages (Supplemental Figure 3, C–F). Therefore, we postulated that the Ras pathway becomes aberrantly activated in endothelial cells during ocular neovascularization, and we predicted that if p120RasGAP levels could be experimentally potentiated (as they do spontaneously in OIR mice) neovascularization could be slowed or prevented.

A candidate regulator of p120RasGAP is miR-132. We have shown that it can directly modulate p120RasGAP expression in vivo by negatively regulating formation of the vasculature in the developing retina and in tumors (22), although its expression pattern and functions preventing ocular neovascularization in the eye have not been determined. Using quantitative RT-PCR (RT-qPCR), we quantified the expression of *Rasa1* mRNA during normal development in isolated neural retinas and showed that its expression steadily increased from P7 to P16 before stabilizing (Figure 3A), and, in the same retinas, miR-132 was expressed in an inverse relationship to *Rasa1* (Figure 3B). In situ hybridization analyses revealed that miR-132 was weakly expressed in neovascular tufts of P18 OIR mice (Supplemental Figure 4). RT-qPCR analyses confirmed that *Rasa1* expression pattern was biphasic and inversely related to miR-132 in OIR mice (Figure 3C), supporting the notion that miR-132 targets this gene (22). These data strongly suggest that miR-132/p120RasGAP signaling contributes to normal and pathological ocular angiogenesis.

α-miR-132 effectively prevents neovascularization. We designed and synthesized chemically stabilized oligonucleotides with sequences complementary to miR-132 (α-miR-132 oligonucleotides). To demonstrate that miRs gain entry to retinal cells, we generated fluorophore-conjugated α-miR-132 constructs. When injected at P12, they were detected preferentially in the GS lectin–posi-

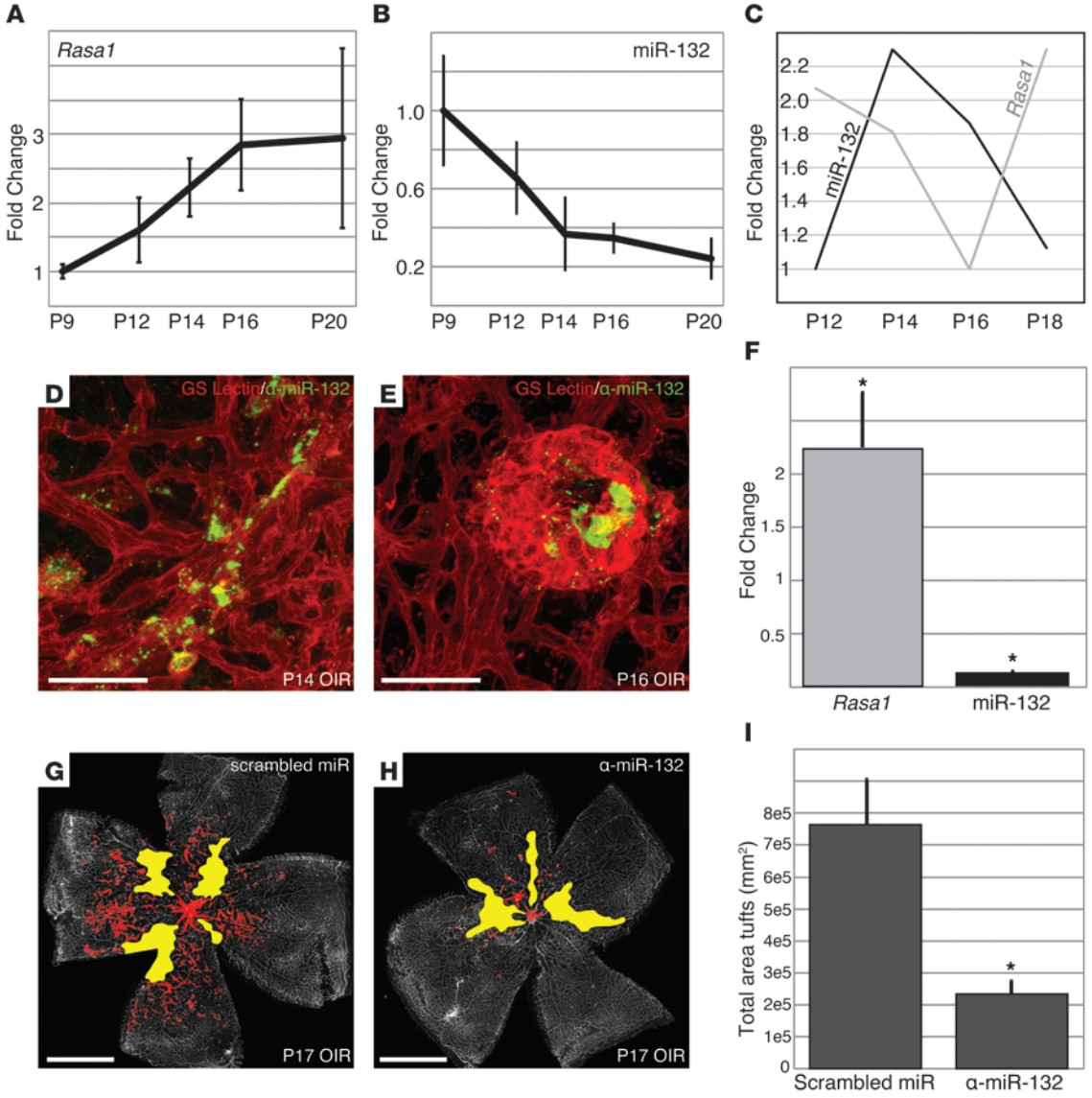

Figure 3

α-miR-132 injections enhance p120RasGAP expression and prevent neovascularization in OIR mice. (**A**) *Rasa1* expression during normal development was quantified using qPCR and plotted in relative values (normalized to *Rasa1* expression levels measured at P9). Note the linear increase until P16 when expression levels saturate. (**B**) miR-132 expression in the same retinas was plotted similarly. Expression of miR-132 is inverted compared with that of *Rasa1*, suggesting that miR-132 negatively regulates p120RasGAP to promote angiogenesis until the vascular networks are constructed. (**C**) Quantification of *Rasa1* and miR-132 in OIR mice. The fold change data were normalized to fit on a 1.0- to 2.3-fold change scale (the actual highest fold change value for both was 2.3 for miR-132 and 2.2 for *Rasa1*). (**D** and **E**) Fluorophore-conjugated α-miR-132 constructs (green) were injected at P12, and the constructs were largely taken up by activated endothelial cells (red) at P14 (**D**) and P16 (**E**). (**F**) qPCR analyses confirm that *Rasa1* is significantly upregulated and miR-132 is downregulated in eyes injected with α-miR-132 (n = 4; *P = 0.04). GS lectin–stained neural retina flat-mount preparations of (**G**) vehicle- and (**H**) α-miR-132–injected retinas isolated from P17 OIR mice. Neovascular tufts and vaso-obliterated regions are labeled red and yellow, respectively. (**I**) Total area of tufts and vaso-obliterated regions in vehicle- and α-miR-132–injected eyes was calculated and plotted (OIR experiments were repeated 6 times with n = 8–13 mice; a representative experiment with n = 12 is shown; *P = 0.001). Scale bars: 50 μm (**D** and **E**); 1 mm (**G** and **H**). Error bars represent SEM.

tive cells (endothelial cells and microglia) and not in retinal neurons at P14 and P16, demonstrating selective targeting (Figure 3, D and E). Importantly, the stabilized miR constructs were deliverable without lipid carriers or mechanical disruption of the cells. RT-qPCR was used to confirm that *Rasa1* and miR-132 were significantly modulated by α-miR-132 at P14 compared with controls (Figure 3F). This modulation of p120RasGAP expression effectively prevented hypoxia-induced neovascularization. The OIR phenotype was quantified to measure the surface area of the neovascular tufts and vaso-obliteration (Figure 3, G and H). A 69.4% (P = 0.001) reduction of tufts was observed in eyes injected with α-miR-132 compared with that in eyes injected with scrambled miRs (Figure 3I). No significant difference was observed in the extent of vaso-obliteration (13.3%, P = 0.4).

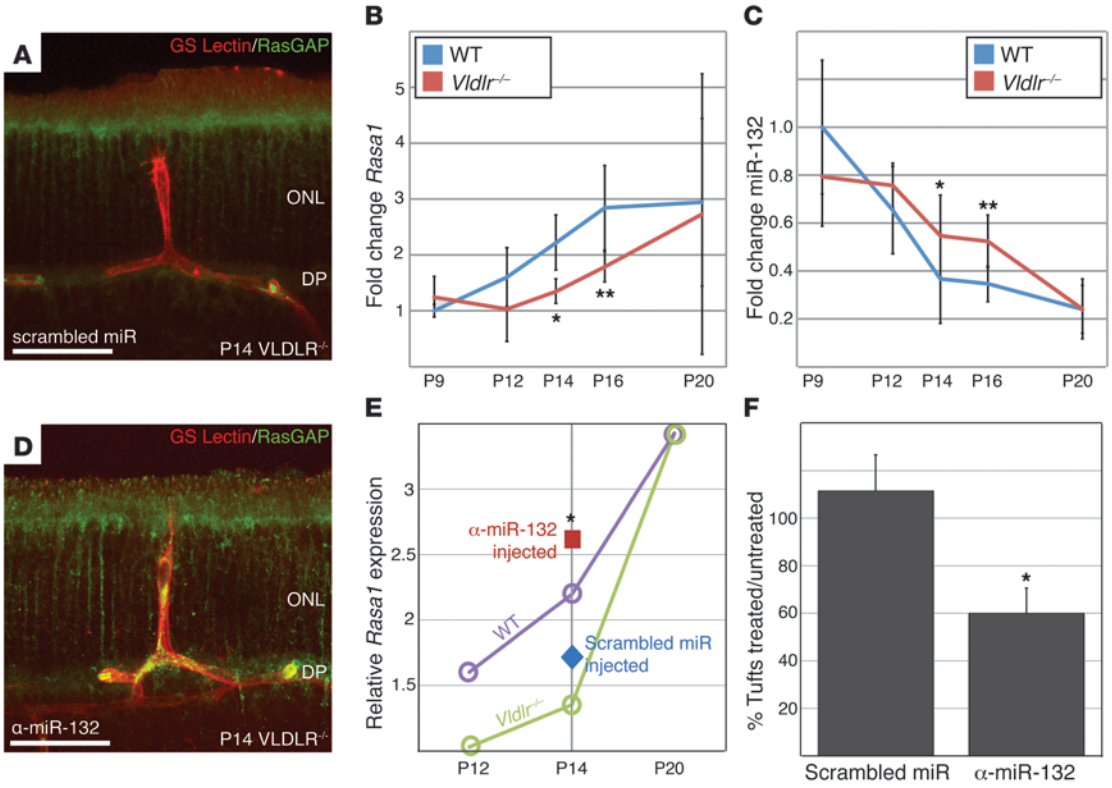

Figure 4

Injections of α-miR-132 result in reduced neovascularization in *Vldlr*$^{-/-}$ mice. (**A**) A thick-cut section of a P14 *Vldlr*$^{-/-}$ retina stained with GS lectin (red) and p120RasGAP (green). qPCR analyses reveal that (**B**) *Rasa1* and (**C**) miR-132 are dysregulated and expressed in inverse patterns in *Vldlr*$^{-/-}$ mice (red lines) at time points when the neovascular tufts develop compared with wild-type mice (blue lines) (P14 $n = 4$, $^{*}P = 0.02$; P16 $n = 4$, $^{**}P = 0.04$). (**D**) Injections of α-miR-132 at P12 results in p120RasGAP (green) upregulation in the angiomas. (**E**) α-miR-132 injections (red square) at P12 nearly restore Rasa1 expression to wild-type levels (purple circle), as compared with vehicle injections (blue diamond) and untreated *Vldlr*$^{-/-}$ mice (green circle). A significant difference was observed in *Vldlr*$^{-/-}$ eyes injected with α-miR-132 and scrambled miR ($n = 4$, $^{*}P = 0.04$). (**F**) The number of tufts in the antagomir-injected eyes was divided by the number of tufts in the uninjected eyes to generate a percentage value for the number of tufts in each animal. These values were averaged and plotted. The averaged percentage of the number of tufts from scrambled miR/uninjected retinas is shown for comparison ($n = 6$, $^{*}P = 0.02$). Scale bars: 50 μm (**A** and **D**). ONL, outer nuclear layer. Error bars represent SEM.

In retinas of P14 *Vldlr*$^{-/-}$ mice, pERK was detected in the sprouting endothelial cells of proliferative angiomas and p120RasGAP was detected at lower levels in *Vldlr*$^{-/-}$ mice (Figure 2, F–H, and Figure 4A). Additionally, from P9 to P20, RT-PCR analyses revealed significant dysregulation of *Rasa1* and miR-132 expression patterns (Figure 4, B and C). P12 *Vldlr*$^{-/-}$ pups were injected with α-miR-132, and p120RasGAP was readily detectable in neovascular sprouts extending into the outer nuclear layer (Figure 4D). α-miR-132 injections restored p120RasGAP to slightly higher levels than those observed in wild-type mouse retinas (Figure 4E).

To determine the effects of potentiating p120RasGAP in *Vldlr*$^{-/-}$ mice, we compared the number of neovascular tufts in each eye after injecting one eye of each animal with α-miR-132 or scrambled miR (the contralateral eye was not injected for comparison). The percentage of the number of angiomas was calculated (α-miR-132 or scrambled miR vs. uninjected) and plotted. We observed only 60% ($P = 0.02$) as many tufts in *Vldlr*$^{-/-}$ mice injected with α-miR-132; no significant difference was observed in *Vldlr*$^{-/-}$ mice injected with scrambled miR when compared with uninjected *Vldlr*$^{-/-}$ mice (Figure 4F). Therefore, potentiating p120RasGAP expression in *Vldlr*$^{-/-}$ mice limited endothelial cell sprouting and significantly reduced neovascularization.

Electroretinography experiments were performed 4 days after injecting α-miR-132 or scrambled miR in wild-type adult mice to ensure that the retinal neurons were not affected by the treatment. No significant difference was detected between the amplitudes of the a- and b-waves from scotopic electroretinography recordings after injecting either scrambled miR or α-miR-132 (Supplemental Figure 5, A–C). No significant differences could be detected in photopic b-waves or flicker responses either (Supplemental Figure 5, D–G). Cone densities were also examined after injection of scrambled miR or α-miR-132 by examining cone red/green opsin expression in flat-mounted retinas 6 days after injection, and no obvious differences were observed (Supplemental Figure 6, A and B). These data suggest that the photoreceptors appear normal and function correctly after injecting α-miR-132, a key finding since we demonstrated previously that cones are more sensitive than rods to vascular changes (1). Last, we also examined the vasculature integrity of wild-type adult retinas injected with scrambled miR or α-miR-132 6 days after injection and observed no gross changes (Supplemental Figure 6, C and D).

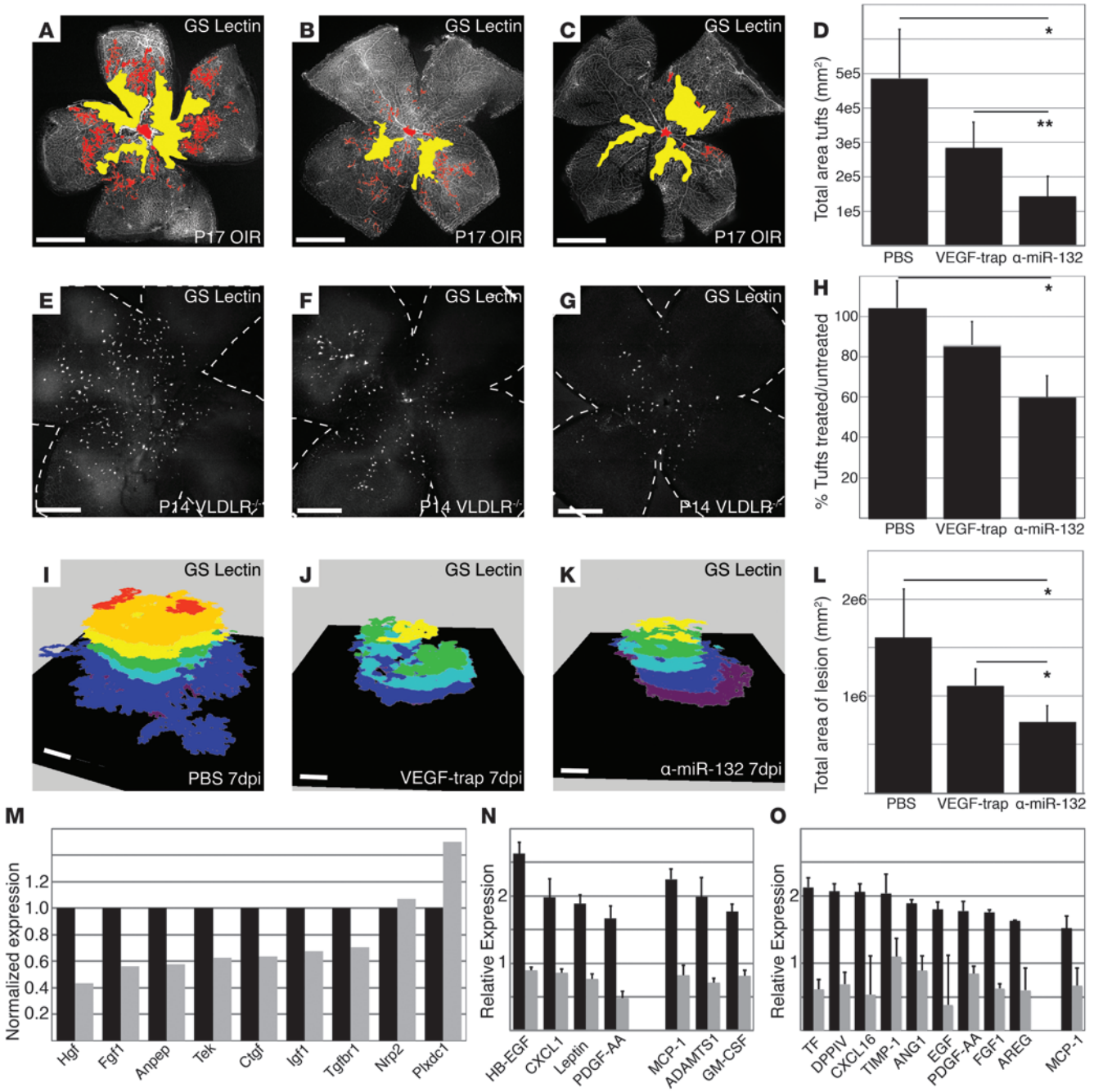

Figure 5

α-miR-132 is more effective than VEGF-trap at reducing neovascularization. Images of superficial plexus from (**A**) vehicle, (**B**) VEGF-trap–, and (**C**) α-miR-132–injected OIR retinas. (**D**) The area of neovascularization for all 3 conditions was plotted (n = 6–8; PBS vs. α-miR-132, $^*P$ = 0.03; VEGF-trap vs. α-miR-132, $^{**}P$ = 0.05). Images of the outer retina from (**E**) vehicle-, (**F**) VEGF-trap–, or (**G**) α-miR-132–injected *Vldlr*$^{-/-}$ mice. (**H**) Percentages of *Vldlr*$^{-/-}$ tufts were calculated from vehicle-, VEGF-trap–, or α-miR-132–injected eyes versus contralateral uninjected eyes (n = 6, $^*P$ = 0.02). Laser-induced lesions in wild-type B6 mice in (**I**) vehicle-, (**J**) VEGF-trap–, or (**K**) α-miR-132–injected eyes were imaged using confocal microscopy (Z stacks = 5 μm). The pixels in the lesions were pseudocolored a different color for distinction. 3D renditions of the lesions were generated to emphasize morphology and depth of the injuries. (**L**) Quantification of the volume of the lesions (PBS vs. α-miR-132 and VEGF-trap vs. α-miR-132, n = 8–20, $^*P$ = 0.04). (**M**) Gene-profiling analyses reveal that most of the genes compensatorily upregulated by VEGF-trap in wild-type B6 retinas are not similarly activated by α-miR-132. (**N** and **O**) Proteome profiling arrays involving various markers of angiogenesis reveal that several angiogenic and proinflammatory proteins (separated with a gap in both plots) are dysregulated in a compensatory manner by VEGF-trap (black columns) but not α-miR-132 injections (gray bars) at (**N**) P15 and (**O**) P17 in OIR mice. Proteins dysregulated by >1.5 fold with P values of less than 0.05 were plotted. Scale bars: 1 mm (**A**–**C** and **E**–**G**); 50 μm (**I**–**K**). Error bars represent SEM.

α-*miR-132 is more effective than VEGF-trap*. VEGF-trap, a fusion protein of IgG Fc fragments and VEGFR1/VEGFR2, has been shown to reduce tuft formation in animal models of OIR and laser-induced choroidal neovascularization (CNV) (23–25) and in patients with age-related macular degeneration with CNV (26, 27). We developed a VEGF-trap mimetic and tested its activity at several doses (Supplemental Figure 7A) and also directly compared its angiostatic activity with that of commercially available aflibercept (Eylea or VEGF-trap Eye) in both the OIR and laser-induced CNV models. We observed no significant difference between the antiangiogenic activities of either drug (Supplemental Figure 7, B and C), validating the use of our VEGF-trap mimetic. We then directly compared the angiostatic activity of α-miR-132 and VEGF-trap in OIR and *Vldlr*$^{-/-}$ mice. α-miR-132 was significantly more potent than VEGF-trap in preventing neovascular tuft formation in OIR mice (Figure 5, A–D) and in reducing the number of angiomas in *Vldlr*$^{-/-}$ mice (Figure 5, E–H).

We also compared the angiostatic activity of VEGF-trap and α-miR-132 in the laser-induced CNV model. Adult mouse eyes were exposed to laser photocoagulation and immediately examined using confocal scanning laser ophthalmoscopy to monitor the extent of the injury. The animals were then intravitreally injected with PBS, VEGF-trap, or α-miR-132. One week later, the eyes were reevaluated using confocal scanning laser ophthalmoscopy coupled with indocyanine green angiography to visualize the choriocapillaris (Supplemental Figure 8, A–C). For quantification, the eyes were enucleated, and the GS lectin–labeled lesions in RPE/choroid flat mounts were imaged using confocal microscopy (Figure 5, I–K; Z-projections of the images are shown in Supplemental Figure 8, D–F). The volume of the lesions was also calculated and plotted (Figure 5L). These data confirm that both VEGF-trap and α-miR-132 effectively inhibit laser-induced CNV but that higher levels of CNV inhibition are obtained when α-miR-132 is used.

Gene-profiling assays were used to assess changes in angiogenic gene expression after treatment with α-miR-132 or VEGF-trap. Compensatory upregulation of angiogenic or inflammatory factors is observed after treatment with antiangiogenic monotherapies that inhibit a single pathway or factor, such as VEGF (28–30). After treating OIR retinas with α-miR-132 or VEGF-trap, we performed RT-PCR with an array of 84 angiogenesis-related genes and multiplex ELISA assays for 55 proteins associated with angiogenesis at P15 or P17. The data were filtered, and only those proteins with *P* values less than or equal to 0.05 were plotted (Figure 5, M–O). Injection of α-miR-132, in general, either had no effect or induced downregulation of the genes and proteins examined. Injections of VEGF-trap, however, induced substantial upregulation of several genes. Those proteins upregulated 1.5 fold or more, with a *P* value less than or equal to 0.05, were plotted (Figure 5N). By P17, VEGF-trap injections induced an increased upregulation of angiogenic proteins, based on the same exclusion criteria (Figure 5O). By comparison, α-miR-132 injection did not induce compensatory upregulation of angiogenic proteins in conditions of hypoxia-induced retinopathy.

Discussion

In this study, we examined the expression patterns of Ras signaling elements in the murine retina during normal postnatal vascular development and pathological neovascularization. pERK was readily detectable in sprouting endothelial cells during development and in models of inner (OIR) and outer (*Vldlr*$^{-/-}$) retinal neovascularization. p120RasGAP was detectable in tip cells in patterns similar to those of UNC5B. UNC5B in tip cells has been shown to prevent endothelial cell sprouting (6), and we suggest that p120RasGAP functions similarly (for a cartoon schematic see Supplemental Figure 9). This assertion is supported by 4 observations: (a) p120RasGAP and UNC5B expression levels were highly enriched in endothelial cells that maintain quiescence, even in the face of high VEGF levels; (b) in OIR mice, p120RasGAP was spontaneously activated at high levels at P18 when the neovascular tufts begin to spontaneously regress (31); (c) the experimental induction of p120RasGAP in the deep plexus and invasive endothelial cells of *Vldlr*$^{-/-}$ mice prevented angioma formation; (d) and α-miR-132–mediated *Rasa1* activation in OIR mice, *Vldlr*$^{-/-}$ mice, and in mice exposed to laser photocoagulation significantly prevented neovascularization. Evidence from the literature also supports the notion that p120RasGAP prevents endothelial cell sprouting, since α-miR-132 inhibits normal vasculature development in the retina (22), and, in humans, *RASA1* mutations are associated with multiple neovascular phenotypes (14–16).

Multiple cytokines, including but not limited to VEGF, converge on the Ras pathway to activate angiogenesis; this may explain why inhibition of Ras signaling with α-miR-132 more potently prevents neovascularization than do VEGF antagonists. However, long-term safety studies are necessary to determine whether chronic intraocular administration of α-miR-132 will lead to any adverse events. While we did not observe any adverse or off-target effects in our rodent studies, miR-132 has been shown to serve important functions in both the brain and immune system (32). Notwithstanding, α-miR-132 is an attractive potential candidate for the treatment of abnormal retinal neovascularization for several reasons: (a) it can be relatively easily delivered using intravitreal injections and does not require viral or lipid carrier–based systems; (b) it is preferentially taken up by endothelial cells in the neovascular front; (c) there are no adverse effects on existing vasculature; and (d) it appears to be even more potent than VEGF-trap in inhibiting abnormal angiogenesis. Furthermore, other groups and our own have shown that strong VEGF antagonism may induce degeneration of preexisting vasculature and neurons (1, 3). Notably, unlike VEGF antagonism, α-miR-132 antagonism does not activate compensatory upregulation of proangiogenic and proinflammatory factors. In conclusion, we propose that limiting VEGF activity through α-miR-132–mediated p120RasGAP activation may be a very effective and safe method for preventing endothelial cell sprouting in a variety of neovascular eye diseases.

Methods

Animal models. C57BL/6 mice used in these studies were treated in adherence with the NIH Guide for the Care and Use of Laboratory Animals. OIR experiments were performed as described previously (33). Eyes were collected at either P15 or P17 for analysis, prepared as flat mounts, and immunolabeled with GS lectin (catalog no. L21416, Invitrogen) for quantification. OIR experiments were quantified using established techniques (31, 34). At least 8 eyes were analyzed per group, and each experiment was repeated at least 3 times.

Vldlr$^{-/-}$ tuft quantification was done by imaging GS lectin–stained flat-mounted retinas at the RPE/retinal interface. The number of tufts in each eye was manually counted using ImageJ software and the CellCounter plug-in (NIH). Since only one of the eyes was treated, the number of angiomas in treated eyes was divided by number of angiomas observed in untreated eyes. The values obtained from each mouse for each different

treatment were averaged and plotted using Excel software (Microsoft). At least 5 mice from at least 2 different litters were compared for this analysis. The groups analyzed included mice injected with PBS, scrambled miR, VEGF-trap, or α-miR-132. For all the assays, paired Student's *t* tests were used to determine statistical significance.

Laser photocoagulation was performed at 4 spots per eye around the optic disk with the wavelength of 532 nm, 200 mW, 100-ms duration, and a spot size of 75 μm using a slit-lamp laser photocoagulation system (Novus Spectra; Lumenis) as previously described (1). One week after laser injury, mice were sacrificed, and RPE/choroid whole mounts were prepared for CNV volume quantification. The pixels were pseudocolored and counted in each Z-stack. The colored layers were combined into a 3D image using PhotoShop CS5 (Adobe) to better visualize the morphology and volume of the lesions.

Intraocular injections and tissue processing. A 33-gauge sharp Hamilton syringe was used to deliver a 0.5 μl volume of each reagent into the vitreous of mouse eyes. Mouse eyes were enucleated, and flat-mount preparations were prepared as described previously after removing the cornea, lens, RPE, choroid, and sclera (4, 35). Primary antibodies raised against p120RasGAP (catalog no. B478; Santa Cruz Biotechnology Inc.), pERK (phospho-p44/42 MAPK, catalog no. 9101; Cell Signaling), UNC5B (catalog no. ab104871; AbCam), VEGFR2 (catalog no. ab2349; AbCAM), cone red/green opsin (catalog no. AB5405; Millipore), and fluorescent-conjugated secondary antibodies (Life Sciences) were used in this study. Samples were mounted in SloFade Gold (Life Sciences). Images were captured at room temperature using a Zeiss 700 inverted confocal microscope (Zeiss) with ×5/0.16, ×10/0.30, ×20/0.8, and ×40/0.95 objective lenses and processed using ImageJ (NIH) and Adobe Photoshop (Adobe). In situ hybridization assays were performed using miRCURY LNA microRNA detection probes (hsa-miR-132 5′DIG labeled, no. 38031-01, and scramble-miR 5′DIG labeled, no. 99004-01) and the reagents recommended by the supplier for their use (Exiqon) and premade hybridization buffer (Enzo) following the manufacturer's directions. BM Purple (Roche) was used for colorimetric development. For double labeling, fluorescent-conjugated GS lectin was mixed with anti-DIG antibodies.

RT-qPCR and ELISA analyses. Total RNA was prepared from retinal tissues using the miRNeasy Mini Kit (Qiagen) and was reverse transcribed using the QuantiTect Reverse Transcription Kit (Qiagen) or the TaqMan MicroRNA Reverse Transcription Kit (Life Technologies). Quantitative PCR assays were performed on a real-time PCR System (ABI 7900HT Fast; Life Technologies) using a PCR master mix (TaqMan Fast Universal or TaqMan Universal PCR Master Mix; Life Technologies) and TaqMan gene expression assay mix of *Rasa1* (Mm00520858_m1) or TaqMan MicroRNA Assays of miR-132 (Assay ID: 000457). Eukaryotic 18S ribosomal RNA TaqMan MGB probe was used as an endogenous control. Data were analyzed with 7900HT Fast System SDS software (version 2.4; Life Technologies). All experiments were performed with 3 replicates. The data were normalized to P9 wild-type *Rasa1* or miR-132, except in the case of the OIR experiments. In the OIR experiments, the data were normalized to P12 wild-type expression levels. The data were then normalized again so that both data sets fit on a 1.0- to 2.3-fold change scale for direct comparison. Proteome Profiler Mouse Antibody Array Kits (R&D Systems) were used for this analysis following the manufacturers instructions, with one modification: IR800-conjugated avidin (Licor) was used. The retinas were isolated from P15 and P17 staged OIR mice injected with PBS, VEGF-trap, scrambled miR, or α-miR-132 (n = 8). Quantification was performed after scanning the membranes on an Odyssey infrared scanner (Licor) using Image Studio software (Licor).

Preparation of α-miR-132 and VEGF-trap. α-miR-132 oligonucleotides were generated as described previously (22); in some cases, Cy3 was conjugated to the 5′ end (Sigma-Aldrich). The oligonucleotides were resuspended in RNAse-free water to a concentration of 100 μM. A VEGF-trap (aflibercept) mimic, a fusion protein of key domains from human VEGFR1 and VEGFR2 with human IgGFc, was made as described previously and shown to be effective for binding and neutralizing murine VEGF (36–38). Briefly, the gene encoding for VEGF-trap, with a carboxy-terminal histidine tag (H6), was cloned into a transposon-based system, and stable cell lines were derived after selection for neomycin resistance (Geneticin, 500 μg/ml). The HEK-293F cells (catalog no. R790-07; Invitrogen) were grown in suspension in Freestyle 293 Expression Media (catalog no. 12338; Life Sciences) at 37°C, 8% CO_2. VEGF-trap protein was purified using IMAC Ni-Charged Resin column purification (catalog no. 156-0131; Bio-Rad). After purification, the recombinant protein was verified by Coomassie blue staining after SDS-PAGE and quantified with a spectrophotometric method. The final storage buffer was 50 mM sodium phosphate, containing 150 mM NaCl (pH 7.0). Eylea was purchased from Bayer. 1.25 μg VEGF-trap was calculated to be an equivalent amount to that injected in human patients (based on the difference between the volume of the vitreous of humans and mice). To ensure that we were not delivering a suboptimal dose, we tested higher and lower dosages of VEGF-trap (2.5 μg, 1.25 μg, and 0.625 μg) in P12 to P17 OIR mice. 1.0 μg α-miR-132 was used in all experiments, although lower dosages were tested (0.5 μg and 0.25 μg).

Statistics. Paired 2-tailed Student's *t* tests were used to determine statistical significance. *P* values of less than 0.05 were considered significant.

Study approval. The present studies in animals were reviewed and approved by the IACUC of The Scripps Research Institute.

Acknowledgments

We would like to thank Mariah Webb, Alison Dorsey, and Matthew Wang for expert technical assistance and Michele Gerhart for administrative support. This work was funded by grants to M. Friedlander from the National Eye Institute (EY022025-01 and EY11254) and the Lowy Medical Research Institute (MacTel). D. Cheresh is supported by NIH grants (CA50286 and HL103956). P.D. Westenskow is a Ruth L. Kirschstein Fellow of the NIH (EY021416). T. Kurihara is supported by a fellowship from the Manpei Suzuki Diabetes Foundation and the Japan Society for the Promotion of Science Postdoctoral Fellowship for Research Abroad.

Received for publication April 3, 2013, and accepted in revised form August 1, 2013.

Address correspondence to: Martin Friedlander, 10550 N. Torrey Pines Rd., La Jolla, California 92037, USA. Phone: 858.784.9138; Fax: 858.784.9135; E-mail: friedlan@scripps.edu.

1. Kurihara T, Westenskow PD, Bravo S, Aguilar E, Friedlander M. Targeted deletion of Vegfa in adult mice induces vision loss. *J Clin Invest*. 2012; 122(11):4213–4217.
2. Saint-Geniez M, Kurihara T, Sekiyama E, Maldonado AE, D'Amore PA. An essential role for RPE-derived soluble VEGF in the maintenance of the choriocapillaris. *Proc Natl Acad Sci U S A*. 2009; 106(44):18751–18756.
3. Eremina V, et al. VEGF inhibition and renal thrombotic microangiopathy. *N Engl J Med*. 2008; 358(11):1129–1136.
4. Dorrell MI, Aguilar E, Friedlander M. Retinal vascular development is mediated by endothelial filopodia, a preexisting astrocytic template and specific R-cadherin adhesion. *Invest Ophthalmol Vis Sci*. 2002;43(11):3500–3510.
5. Gerhardt H, et al. VEGF guides angiogenic sprouting utilizing endothelial tip cell filopodia. *J Cell Biol*. 2003;161(6):1163–1177.
6. Mazzone M, et al. Heterozygous deficiency of PHD2 restores tumor oxygenation and inhibits metastasis via endothelial normalization. *Cell*. 2009; 136(5):839–851.
7. Jakobsson L, et al. Endothelial cells dynamically compete for the tip cell position during angiogenic sprouting. *Nat Cell Biol*. 2010;12(10):943–953.

8. Lu X, et al. The netrin receptor UNC5B mediates guidance events controlling morphogenesis of the vascular system. *Nature*. 2004;432(7014):179–186.
9. Siekmann AF, Lawson ND. Notch signalling limits angiogenic cell behaviour in developing zebrafish arteries. *Nature*. 2007;445(7129):781–784.
10. Suchting S, et al. The Notch ligand Delta-like 4 negatively regulates endothelial tip cell formation and vessel branching. *Proc Natl Acad Sci U S A*. 2007; 104(9):3225–3230.
11. Meadows KN, Bryant P, Pumiglia K. Vascular endothelial growth factor induction of the angiogenic phenotype requires Ras activation. *J Biol Chem*. 2001;276(52):49289–49298.
12. McCormick F. ras GTPase activating protein: signal transmitter and signal terminator. *Cell*. 1989; 56(1):5–8.
13. Henkemeyer M, et al. Vascular system defects and neuronal apoptosis in mice lacking Ras GTPase-activating protein. *Nature*. 1995;377(6551):695–701.
14. Boon LM, Mulliken JB, Vikkula M. RASA1: variable phenotype with capillary and arteriovenous malformations. *Curr Opin Genet Dev*. 2005;15(3):265–269.
15. Eerola I, et al. Capillary malformation-arteriovenous malformation, a new clinical and genetic disorder caused by RASA1 mutations. *Am J Hum Genet*. 2003;73(6):1240–1249.
16. Revencu N, et al. Parkes Weber syndrome, vein of Galen aneurysmal malformation, and other fast-flow vascular anomalies are caused by RASA1 mutations. *Hum Mutat*. 2008;29(7):959–965.
17. Stahl A, et al. The mouse retina as an angiogenesis model. *Invest Ophthalmol Vis Sci*. 2010; 51(6):2813–2826.
18. Larrivee B, et al. Activation of the UNC5B receptor by Netrin-1 inhibits sprouting angiogenesis. *Genes Dev*. 2007;21(19):2433–2447.
19. Dorrell MI, et al. Antioxidant or neurotrophic factor treatment preserves function in a mouse model of neovascularization-associated oxidative stress. *J Clin Invest*. 2009;119(3):611–623.
20. Heckenlively JR, et al. Mouse model of subretinal neovascularization with choroidal anastomosis. *Retina*. 2003;23(4):518–522.
21. Le YZ, et al. Inducible expression of cre recombinase in the retinal pigmented epithelium. *Invest Ophthalmol Vis Sci*. 2008;49(3):1248–1253.
22. Anand S, et al. MicroRNA-132-mediated loss of p120RasGAP activates the endothelium to facilitate pathological angiogenesis. *Nat Med*. 2010; 16(8):909–914.
23. Cao J, et al. A subretinal matrigel rat choroidal neovascularization (CNV) model and inhibition of CNV and associated inflammation and fibrosis by VEGF trap. *Invest Ophthalmol Vis Sci*. 2010; 51(11):6009–6017.
24. Jung K, et al. Double anti-angiogenic and anti-inflammatory protein Vα targeting VEGF-A and TNF-α in retinopathy and psoriasis. *J Biol Chem*. 2011;286(16):14410–14418.
25. Lutty GA, McLeod DS, Bhutto I, Wiegand SJ. Effect of VEGF trap on normal retinal vascular development and oxygen-induced retinopathy in the dog. *Invest Ophthalmol Vis Sci*. 2011;52(7):4039–4047.
26. Brown DM, et al. Primary endpoint results of a phase II study of vascular endothelial growth factor trap-eye in wet age-related macular degeneration. *Ophthalmology*. 2011;118(6):1089–1097.
27. Stewart MW, Grippon S, Kirkpatrick P. Aflibercept. *Nat Rev Drug Discov*. 2012;11(4):269–270.
28. Batchelor TT, et al. AZD2171, a pan-VEGF receptor tyrosine kinase inhibitor, normalizes tumor vasculature and alleviates edema in glioblastoma patients. *Cancer Cell*. 2007;11(1):83–95.
29. Bergers G, Hanahan D. Modes of resistance to anti-angiogenic therapy. *Nat Rev Cancer*. 2008; 8(8):592–603.
30. Dorrell MI, Aguilar E, Scheppke L, Barnett FH, Friedlander M. Combination angiostatic therapy completely inhibits ocular and tumor angiogenesis. *Proc Natl Acad Sci U S A*. 2007;104(3):967–972.
31. Banin E, et al. T2-TrpRS inhibits preretinal neovascularization and enhances physiological vascular regrowth in OIR as assessed by a new method of quantification. *Invest Ophthalmol Vis Sci*. 2006; 47(5):2125–2134.
32. Wanet A, Tacheny A, Arnould T, Renard P. miR-212/132 expression and functions: within and beyond the neuronal compartment. *Nucleic Acids Res*. 2012;40(11):4742–4753.
33. Smith LE, et al. Oxygen-induced retinopathy in the mouse. *Invest Ophthalmol Vis Sci*. 1994;35(1):101–111.
34. Connor KM, et al. Quantification of oxygen-induced retinopathy in the mouse: a model of vessel loss, vessel regrowth and pathological angiogenesis. *Nat Protocols*. 2009;4(11):1565–1573.
35. Weidemann A, et al. Astrocyte hypoxic response is essential for pathological but not developmental angiogenesis of the retina. *Glia*. 2010; 58(10):1177–1185.
36. Holash J, et al. VEGF-Trap: a VEGF blocker with potent antitumor effects. *Proc Natl Acad Sci U S A*. 2002;99(17):11393–11398.
37. Koh YJ, et al. Double antiangiogenic protein, DAAP, targeting VEGF-A and angiopoietins in tumor angiogenesis, metastasis, and vascular leakage. *Cancer Cell*. 2010;18(2):171–184.
38. Li Z, Michael IP, Zhou D, Nagy A, Rini JM. Simple piggyBac transposon-based mammalian cell expression system for inducible protein production. *Proc Natl Acad Sci U S A*. 2013;110(13):5004–5009.